Very accurate cryogenic mechanisms for CRIRES+

Lizon, Jean Louis, Klein, Barbara, Molina-Conde, Ignacio, Oliva, Ernesto, Anglada Escude, Guillem, et al.

Jean Louis Lizon, Barbara Klein, Ignacio Molina-Conde, Ernesto Oliva, Guillem Anglada Escude, Paul Bristow, Reinhold J. Dorn, Roman Follert, Artie Hatzes, Ulrike Heiter, Derek Ives, Yves Jung, Matt Lockhart, Thomas Marquart, Livia Origlia, Luca Pasquini, Jerome Paufique, Nikolai Pistunov, Ansgar Reiners, Alain Smette, Jonathan Smoker, Ulf Seemann, Eric Stempels, Elena Valenti, "Very accurate cryogenic mechanisms for CRIRES+," Proc. SPIE 10701, Optical and Infrared Interferometry and Imaging VI, 107012R (9 July 2018); doi: 10.1117/12.2314483

Event: SPIE Astronomical Telescopes + Instrumentation, 2018, Austin, Texas, United States

Very accurate cryogenic mechanisms for CRIRES+

Jean Louis Lizon*[a], Barbara Klein[a], Ignacio Molina-Conde[a], Ernesto Oliva[e], Guillem Anglada Escude[c], Paul Bristow[a], Reinhold J. Dorn[a], Roman Follert[b], Artie Hatzes[b], Ulrike Heiter[d], Derek Ives[a], Yves Jung[a], Matt Lockhart[a], Thomas Marquart[d], Livia Origlia[f], Luca Pasquini[a] ,Jerome Paufique[a], Nikolai Pistunov[e], Ansgar Reiners[c], Alain Smette[a] , Jonathan Smoker[a], Ulf Seemann[c], Eric Stempels[e] , Elena Valenti[a]

[a]European Organisation for Astronomical Research in the Southern Hemisphere, Karl-Schwarzschild Str. 2, D-85748 Garching b. München, Germany;
[b]Thüringer Landessternwarte Tautenburg, Sternwarte 5, D-07778 Tautenburg, Germany;

[c]Institut für Astronomie, Universität Göttingen, Friedrich-Hund-Platz 1, D-37077 Göttingen, Germany;

[d]Department for Physics and Astronomy, Uppsala Universitet, Box 516, S-75120 Uppsala, Sweden; [e]INAF-Osservatorio di Arcetri, Largo E. Fermi 5, I-50125 Firenze, Italy; [f]INAF-Osservatorio di Bologna, via Ranzani 1, I-40127 Bologna, Itali.

ABSTRACT

After 5 years of operation on the VLT, a large upgrade of CRIRES (the ESO Cryogenic InfraRed Echelle Spectrograph) was decided mainly in order to increase the efficiency. Using a cross dispersion design allows better wavelength coverage per exposure. This means a complete re-design of the cryogenic pre-optic which were including a pre-dispersion stage with a large prism as dispersive element.
The new design requires a move of the entrance slit and associated decker toward the first intermediate focal plane right behind the window. Implement 2 functions with high positioning accuracy in a pre-defined and limited space was a real challenge. The design and the test results recorded in the ESO Cryogenic Test Facility are reported in this paper.
The second critical function is the grating wheel which positions the 6 cross disperser gratings into the beam. The paper describes the design of the mechanism which includes a detente system in order to guaranty the 5 arc sec positioning reproducibility requested. The design includes also feedback system, based on switches, in order to ensure that the right grating is in position before starting a long exposure.
The paper reports on the tests carried out at cryogenic temperature at the sub-system level. It also includes early performances recorded in the instrument along the first phases of the system test.

Keywords: Cryogenic mechanism, Spectrograph, InfraRed instrument.

1. INTRODUCTION

The CRIRES upgrade includes a complete re-design of the pre-disperser unit. The original version known as oCRIRES uses a real pre-dispersion along the main dispersion. The pre-dispersion was provided by a prism while the main dispersion is provided by an echelle grating. The pre-dispersion stage has been completely re-designed into a crossed dispersion system. This has been achieved moving the entrance slit in the first intermediate focal plane and implementing a wheel accommodating 6 Gratings used in cross dispersion.
The present paper only reports on the two most critical modules: the grating wheel which requires a relatively high positioning reproducibility and the slit decker unit which requires a very high positioning accuracy in order to keep the wavelength calibration.

* jlizon@eso.org; phone 0049 8932006780; fax 0049 8932006457; www.eso.org

Optical and Infrared Interferometry and Imaging VI, edited by Michelle J. Creech-Eakman, Peter G. Tuthill, Antoine Mérand, Proc. of SPIE Vol. 10701, 107012R · © 2018 SPIE
CCC code: 0277-786X/18/$18 · doi: 10.1117/12.2314483

2. SLIT AND DECKER UNIT

2.1 Design

The location of the slit unit together with the high positioning accuracy made the design of this unit rather challenging. The slit and decker (two different mechanisms) are placed directly in the first intermediate focal plane right behind the warm pre-optic adaptive optic module. The slit is then slightly outside the cylindrical envelope of the vacuum vessel in a sort of protrusion which is closed by the dichroic entrance window which reflect the visible part of the beam into the AO wave-front sensor. Figure 1 shows the implementation of the slit which is clearly outside the two level of shielding absolutely necessary for this type of Spectrograph operating at wavelength up to 5 microns. This geometric position limit dramatically the space to implement a drive mechanism. This has been solved pushing the motor inside the shields and using arm lever to activate the 2 plates.

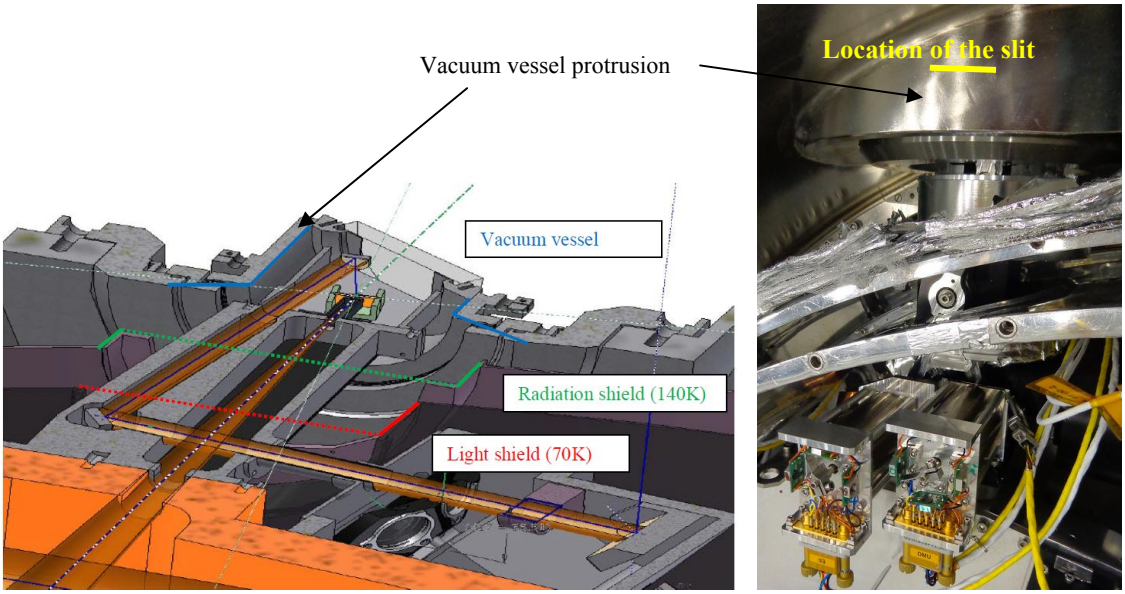

Figure 1. Geometric implementation of the Slit/Decker unit.

The slit and decker are 2 plates which ideally shall be in the focal plane or as close as possible to the focal plane. The two units uses the same principle shown for the slit in Figure 2. Each mask plate is mounted inside a stainless steel frame which is guided in translation by a set of flexural bearings. The motions required in order to perfectly enclosed and define the optical beam for any configurations are +/- 3mm for the slit and +/- 2 mm for the decker plate. Due to the very limited space it was not possible to expend and develop the blades of the flex bearing in order to avoid any early fatigue. A special arrangement have been used folding the flex plate in a M shape.

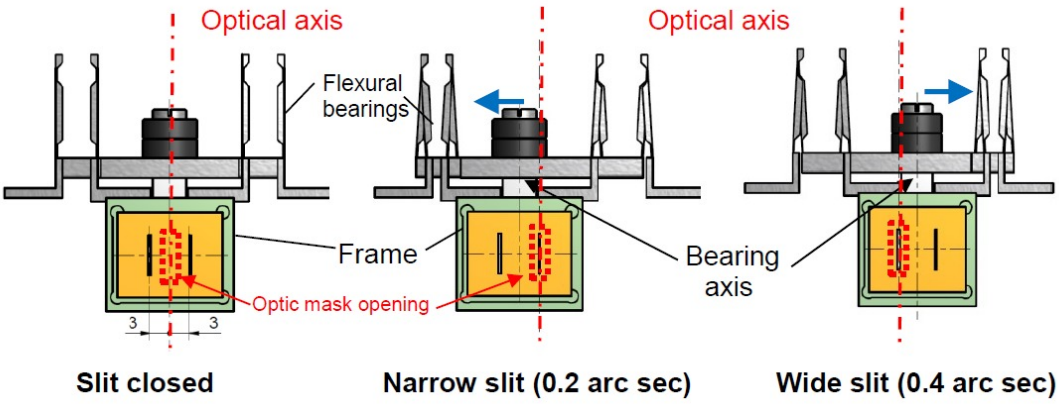

Figure 2. Principle of the slit/decker mechanism.

The motion mechanism (Fig. 3) is rather primitive: The motor (5) (a stepper motor from Phytron adapted to operate at 65K) is equipped with a ~30mm arm which is fitted with a bearing box (4) onto which a small traction spring (3) is hooked. The second side of the spring is hooked onto a second bearing box mounted at the end of the actuator arm (2). The two actuator arms (2 for the decker blade and 10 for the slit plate) are guided by a combination of bearing and axis (16) mounted on the center of the main structure (1). A fork shape manufactured at the end of each actuator arm allows the arm to move the respective frame via a set of ball bearing (13).

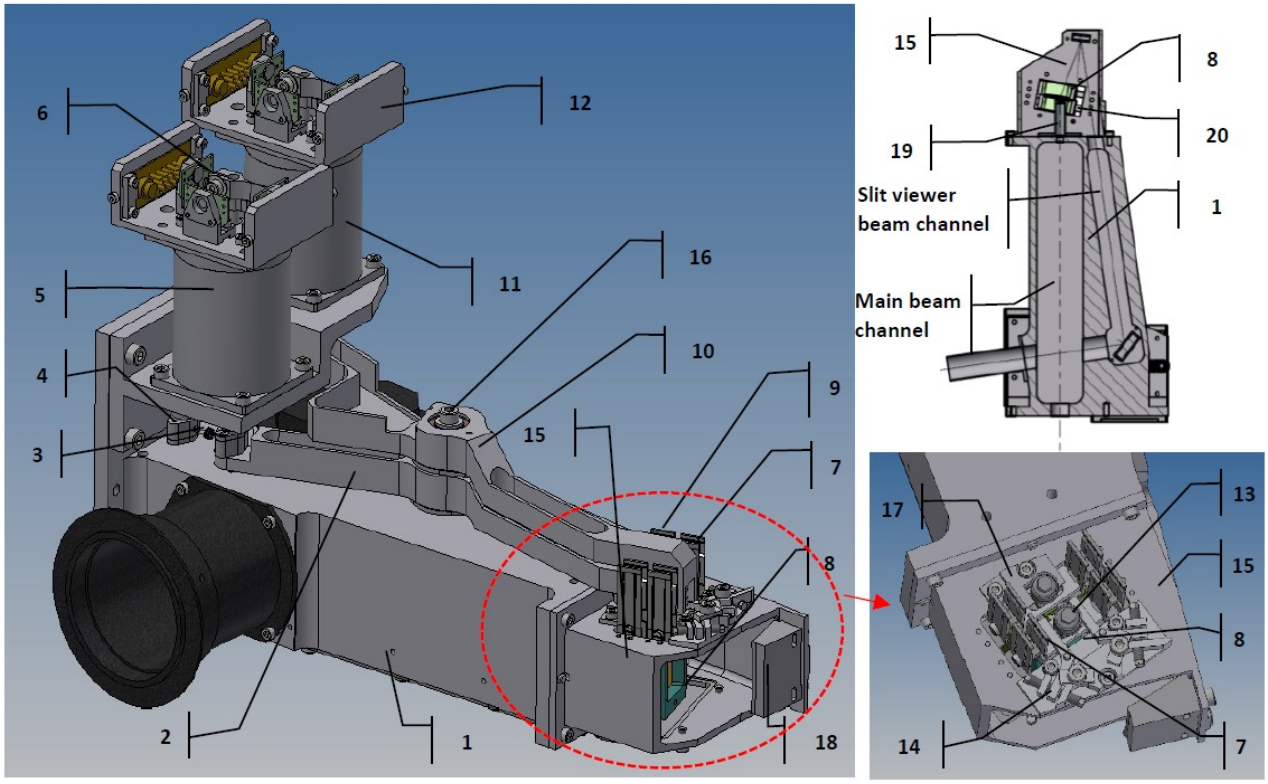

Figure 3. Mechanical design of the slit/decker unit.; (1); Slit/Decker structure; (2): Decker actuator arm; (3); Motion spring for the Decker; (4): Bearing box arm Decker; (5): Decker motor; (6): Limit switch system for Decker; (7): Flex bearing slit; (8): Slit frame; (9): Flex bearing Decker; (10): Actuator arm Decker; (11): Slit motor; (12): Limit box slit; (13): Frame antifriction ball bearing for the slit; (14): Slit position adjustment; (15): Slit module front extension; (16): Arm axis; (17): Mechanical stop Decker: (18): 1st slit viewer mirror; (19): Optical mask; (20): Decker frame.

For practical reasons and in order to ease the manufacturing, the two plate mechanisms are mounted on an extension (15) of the main structure. This extension carries also the first mirror (18) of the slit viewer system. The other optical components are carried by the main structure (1) in a separated dedicated channel machined directly in this structure. The position of the slit plate (2 accurate positions) are defined by two mechanical end stops which position can be adjusted using fine threaded screws (14). The decker plates which only limits the height of the slit does not require the same high accuracy. Therefore the two extreme positions are defined by a fix plate (17). This design allows basically a very high positioning reproducibility for the 2 extreme position which are directly depending on the contact interface at the end stops and the ratio of the forces. Only the decker plate has three real setting positions. The width of the central window of the decker plate will be defined directly from the positioning accuracy of the middle position of the decker frame.

Figure 4 shows a view of the slit and decker frame fully equipped. We can see, between the flex bearings, the pushing axis with the pair of angular contact ball bearing in order to minimize the friction with the actuator arms. These ball bearings as well as all ball bearings included in this unit have been specially prepared in order to be compatible with a cryo-vacuum application. The decker mask is laser cut in an invar plates (direct heritage from VIMOS MOS plate), the slit plate has been manufactured by ion cutting in a silicon plate by Fraunhofer Institute. This technology guaranty an

excellent quality and specially (what is extremely difficult with other traditional manufacturing process) a very accurate slit having extremely sharp wedges. The front surface of the slit is gold coating, it acts as a mirror for the slit viewer beam.

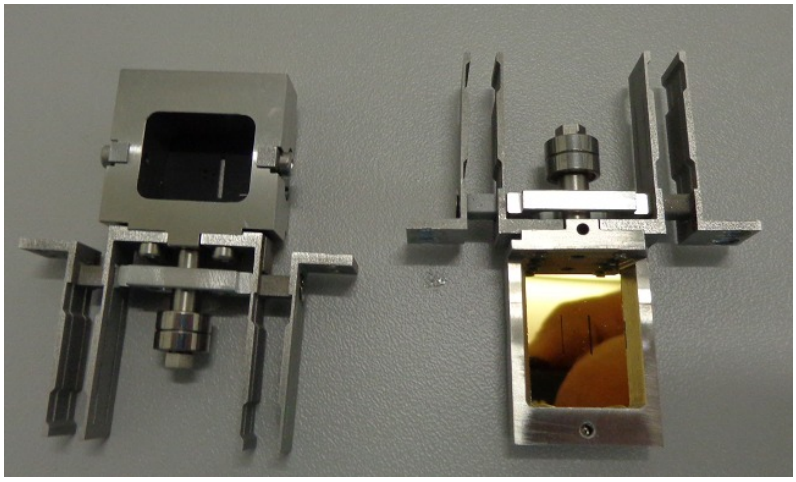

Figure 4. Decker frame on the flex bearing (left), Slit plate on the flex bearings (right).

Figure 5 presents two views of the slit/decker unit partially integrated. On these two pictures we can clearly see the fork shape of the actuator arm enclosing the bearing system of the slit frame.

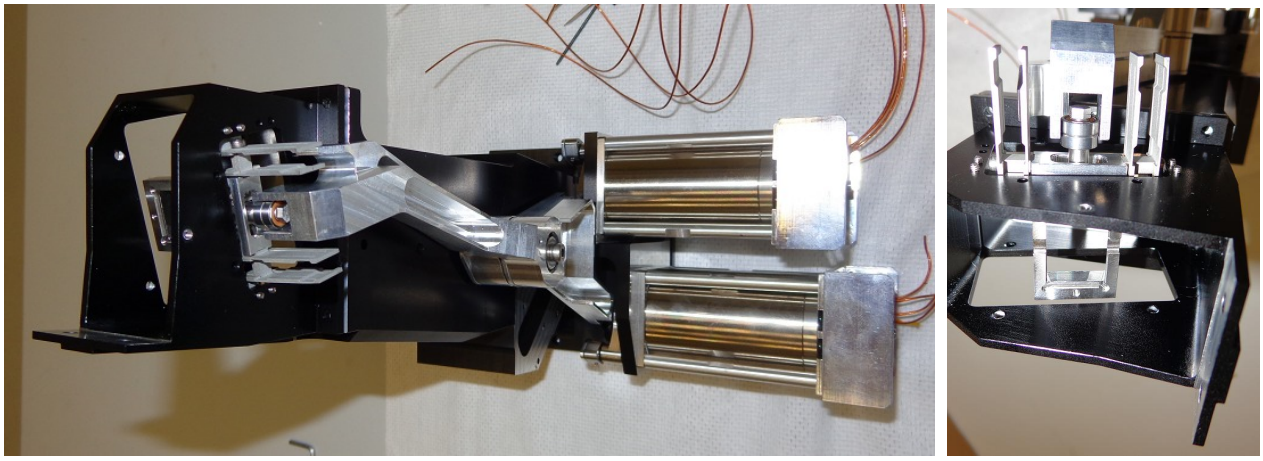

Figure 5. Assembled slit/decker unit (left side) and detail of the front extension (right side).

2.2 Performances

The unit has been integrated with great cares. Every force has been measured and properly adjusted. Then after a few operation test at room temperature, the unit has been installed in the ESO Cryogenic Test Facility (ECFT) which allows a cooling down to 55K. The positioning reproducibility has been measured using 2 commercial inductive transducers from TESA. The transducers are kept inside the ECTF but attached to the warm bench and therefore thermally insulated using contact tip out of G10. For this test the extension structure has been replaced by a test parts with two holes providing feedthrough toward the slit and/or decker frame for the sensors. Figure 6 shows two views of the test setup where we see the insulating tips of the 2 measuring transducers.

Measured in these conditions (Fig.7) at an operating temperature of 55K the slit shows a positioning reproducibility better than 2 microns peak to peak. Very similar performances are measured on the two extreme positions of the decker frame. Figure 8 shows the measurement carried out on the intermediate position of the decker frame. There the real position of the frame is a sort of equilibrium between the various forces. There is nothing to mark and hardly define the

position. The measurements shows a rather important difference depending if the unit is driven from one side or from the other. Nevertheless the positioning error in any case remains always inside 400microns. This means that if the decker is fitted with a middle window (for polarimetry A) of a 800 microns width, the operation shall be safe and fully free of vignetting. Similar measurement performed on the slit frame has shown the same results.

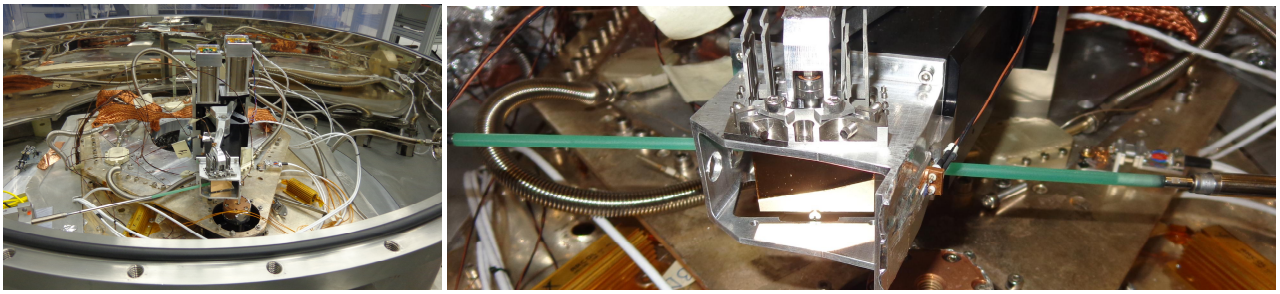

Figure 6. Test set-up in the ESO cryogenic Test Facility.

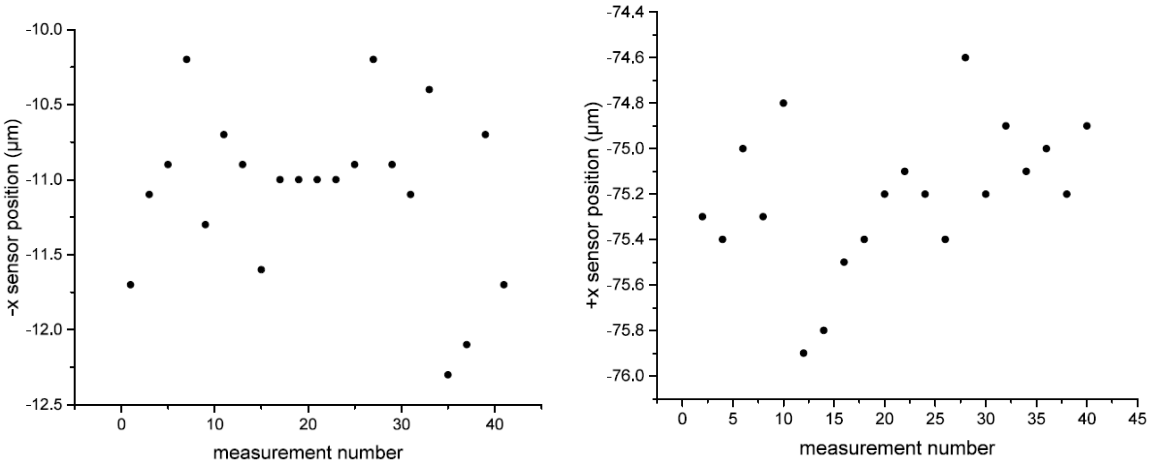

Figure 7. Principle of the slit/decker mechanism.

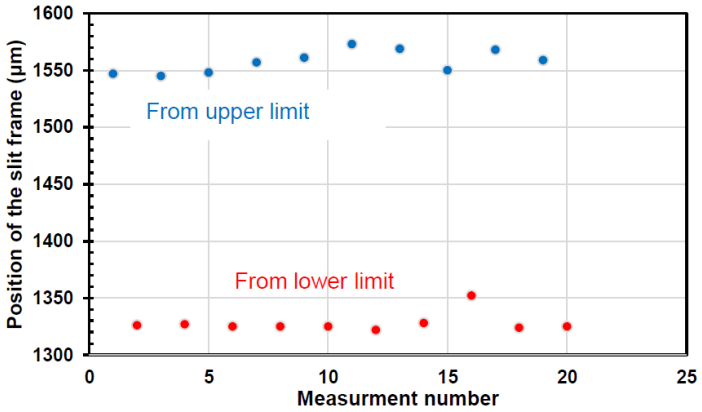

Figure 8. Positioning reproducibility of the intermediate decker position.

2.3 Slit decker unit in the instrument

As documented above, the unit has been tested at the sub-system level in the ECTF at cryogenic temperature. The test has been carried out as usual in two phase including a warming up in-between in order to also assess specific problems

which could be mask in a first operation. Despite this deep testing, two major problems have been encountered during the first test inside the instruments.

As explained at the beginning of this section, the slit is located in a very complex environment and is extending through the various shields. The first problem have been directly caused by a collision between the radiation shield which due to deformation at cryogenic temperature was pressing the actuator arm of the slit.

The second problem was slightly more difficult to identify and fully understand. Also due to its position and especially its location right behind the window, the complete unit is suffering from a serious thermal gradient. The slit frame is operating at a temperature of 80K, which is enough for thermal performance of the spectrograph. On the other hand the actuator arms are operating at much lower temperatures (around 60K). This difference of temperature lead to a shrinkage of the arm fork (made out of Al alloy) onto the ball bearing (stainless steel). A small widening of the fork was necessary to solve this problem, which was not detected in the ECTF where the complete unit was at homogeneous temperature.

Further test carried out during the various optical alignment cool-down has shown a perfect and reliable operation of the two functions.

3. GRATING WHEEL

3.1 Design

Figure 9 show 2 different views of the grating wheel. The 6 gratings and a test mirror (1) are packed in small boxes which are arranged around the grating carousel (2) with the pre-determined angle defined by the blaze angle of each grating. Figure 10 (left side) shows a cut through the grating wheel unit where we can see the two mechanisms used to drive and accurately position the grating in the optical beam. The grating carrousel (2) is mounted onto the base frame (5) guided in rotation using a pair of pre-loaded bearings. The mounting of the bearing is done in the ESO classical way with one bearing (7_1) fully pressed on the martensitic steel axis (22). The second bearing (7_2) is mounted spring-loaded on the diameter and is also pressed axially with the wave washer (8) and the flange (9). The bearing has been fitted with tungsten carbide balls while the races has been gold coated. All these preparations as well as a MoS2 coating of the ball separator and a long run–in leads to a perfectly suitable ball bearing having a reasonable thermal conductance (0.7 W/K) and a relatively low friction torque at cryogenic temperature (0.1 Nm). For this specific application a bearing having less but bigger ball has been selected. This in order to favorize the torque at the cost of a slightly lower thermal performance. A stepper motor from Phytron which develops a torque of 0.25 Nm at cryogenic temperature is used to drive the rotation of the carousel via a pinion / teeth wheel combination. The pinion is manufactured out of Vespel SP3 while the teeth wheel is directly cut in the aluminium carrousel. The reduction ratio is 1/7 in order to have one full motor revolution to go from one grating position to the next one. This allows a permanent verification signal given by the motor sensor actuator (23). A combination of 3 additional sensors (25) and actuators (26) distributed around the wheel is used to verify that the right grating is in position in the beam.

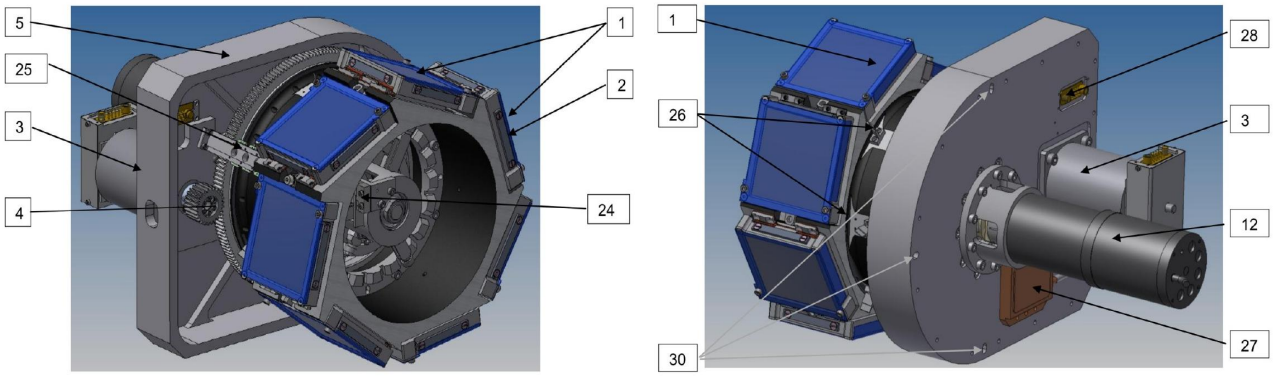

Figure 9. 3D views of the grating wheel unit. 1: grating mount; 2: Grating carousel; (3): rotation motor; (4): Pinion gear; (5): Main frame; (12): locking motor; (24): locking limit switch; (25): Position detection switches; (26): Position detection actuators; (27): LN2 heat exchanger; (28): Electric connector feed through the structure; (30): interface reference slots

A second mechanism is used to lock the carousel in a fixed position with a very high repeatability. The locking is provided by a double tripod cross (6). Three arms of the cross fitted with small ball bearings (15) engaged in three V-grooves which are manufactured in the reference piece (13) which is directly part of the base plate of the function. This defines an absolute position for the locking cross. The locking cross has three additional arms which are equipped with small ball bearings (16). While engaging in the V-slots (14) of the carousel reference piece, which are mounted on the carrousel, the cross will push the carrousel into position. The three long arms are manufactured such that a given flexibility allows for full adaptation along the rotation axis. The locking itself is ensured by a set of tension springs (21) pulling the cross in position with a force of 100N. An interlock system is required in order to verify the release of the lock before rotating the carousel. The following additional mechanism is used for this operation. A screw (11) with a nut (18) fitted with recycled rollers is used to push the cross away from the locking position. The screw is rotated by a combination of stepper motor harmonic drive from Phytron. The torque (rather high ~ 25 Nm) is transmitted to the screw via a custom made Oldham coupling (20). The small bearing (17) guided in a slot of the reference part (13) is used to prevent any rotation of the nut. A limit end switch (24) is used to stop the motion when the locking cross is fully dis-engaged.
The left view of Figure 9 shows a 3D view of the unit where we see the interface with the Cross Dispersion Unit (CDU) structure. Some of the components already described before can be seen on this view. In addition, we see the 3 slots (30) which guarantee a good positioning on the CDU structure fitted with 3 pins. The connector (28) ensures a light tight feed through of the coding signal. The connector for the locking system is still missing from this view. A dedicated heat exchanger (27) is installed on this heavy and critical unit in order to ensure a cool down homogenized with the cooling of the whole instrument. A special cover (14) can be installed on the unit in order to protect the gratings during handling. This is especially important, as the installation is not really simple due to the space constraints.

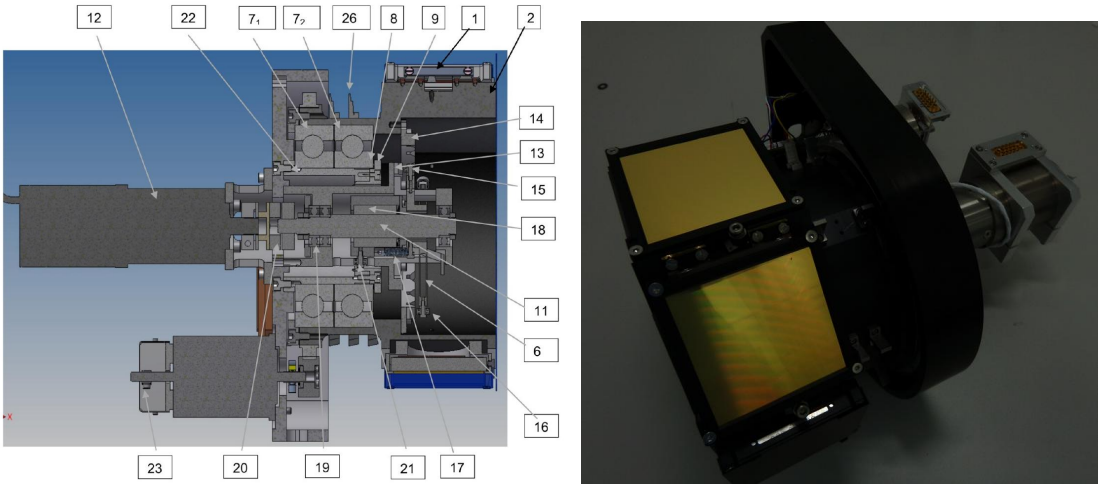

Figure 10. Cut through the grating unit and locking system (left), the complete assembled grating wheel (right). 1: grating mount; 2: Grating carousel; (3): rotation motor; (4): Pinion gear; (5): Main frame; (6): Tripod cross; (7) Ball bearings; (8): Spring washers; (9): Flange; (11): Roller screw spindle; (12): locking motor; (13): Reference piece; (14): Carrousel reference Ve slot; (15): Locking ball bearings, carousel; (16): Locking bearing refence; (17): Translation guide bearing; (18): Roller pre-loaded nut; (19): Spindel ball bearings; (20): Oldham coupling; (21): locking springs; (22): Main axis; (23): Motor sensor actuator; (24): locking limit switch; (25): Position detection switches; (26): Position detection actuators; (27): LN2 heat exchanger; (28): Electric connector feed through the structure; (30): interface reference slots

3.2 Performances

As already mentioned above, the integration phase of this unit requires also a number of testing and specific measurments of forces and torque at the component level. Then the fully integrated unit has been installed in the ECTF (Fig.11) for a long series of measurements. For the test, the unit is fitted with 3 mirrors, the angular position of these mirrors is measured with a Elcomat autocollimator from Moeller Wedel. The full qualification of the unit has been

carried out along a period of 3 weeks during which the units has been cool-down 3 times. The unit has been intensively exercised, the position of the mirrors has been recorded during a number of sequences of 50 positionings. Figure 12 shows a set of measurements recorded during of this measurement campaigns. This set of measurement shows a angular reproducibility better than 2 arc sec (α). The very low dispersion around the second axis (β) has to be accounted to the ball bearing.

Table 1 gives a summary of the performance measured at cryogenic temperature. The slight non conformance of the stability can be caused by a general un-stability of the set-up. A one degree change of temperature of the laboratory can already cause this level of motion.

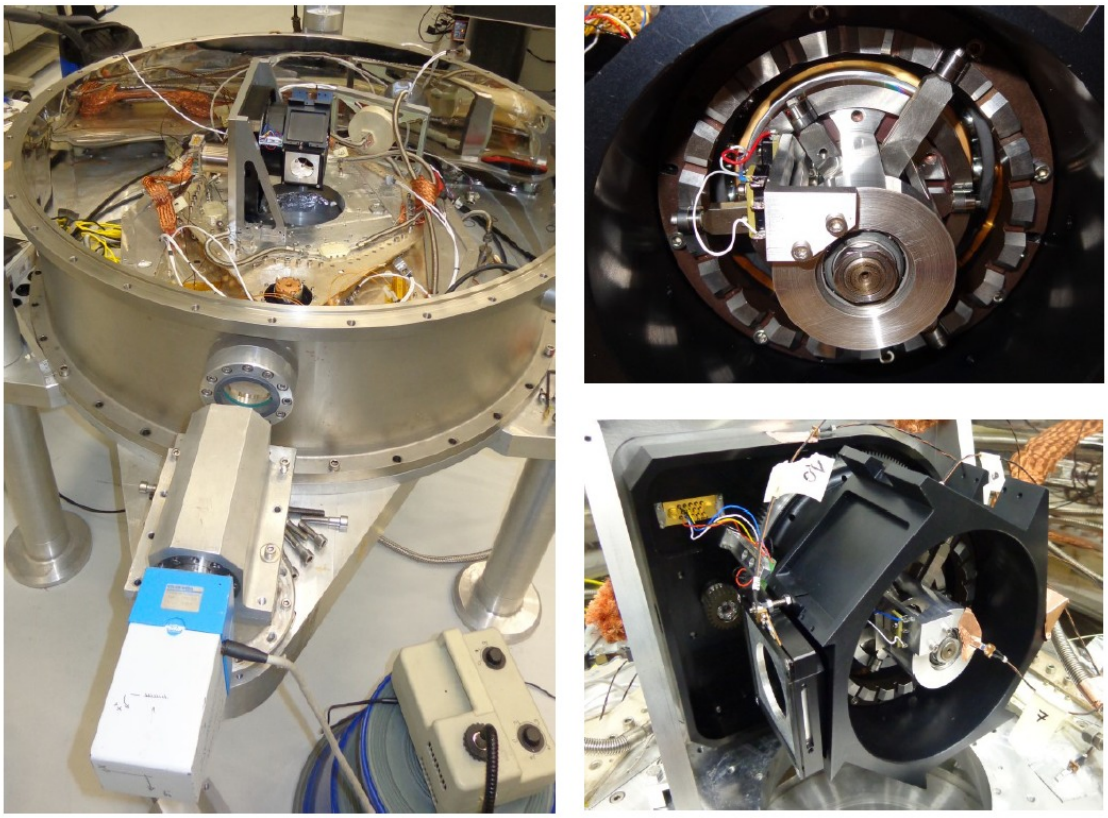

Figure 11. Test set-up of the grating wheel in the ESO Cryogenic Test Facility.

Table 1. Performance of the grating wheel.

	Repeatability		**Stability (4hrs)**	
	Specification:	Measured:	Specification:	Measured:
Wheel rotation **(α)** (cross dispersion direction)	< 4.5 arc sec	**2.5 arc sec p/p**	< 0.5 arc sec	**0.55 P/P**
Parallel to rotation axis **(β)** (main dispersion)	< 2 arc sec	**0.4 arc sec p/p**	< 0.23 arc sec	**0.25 P/P**
Normal to the grating surface **(ɣ)**	< 9 arc sec	Not measured But similar to **β**	< 1 arc sec	Not measured

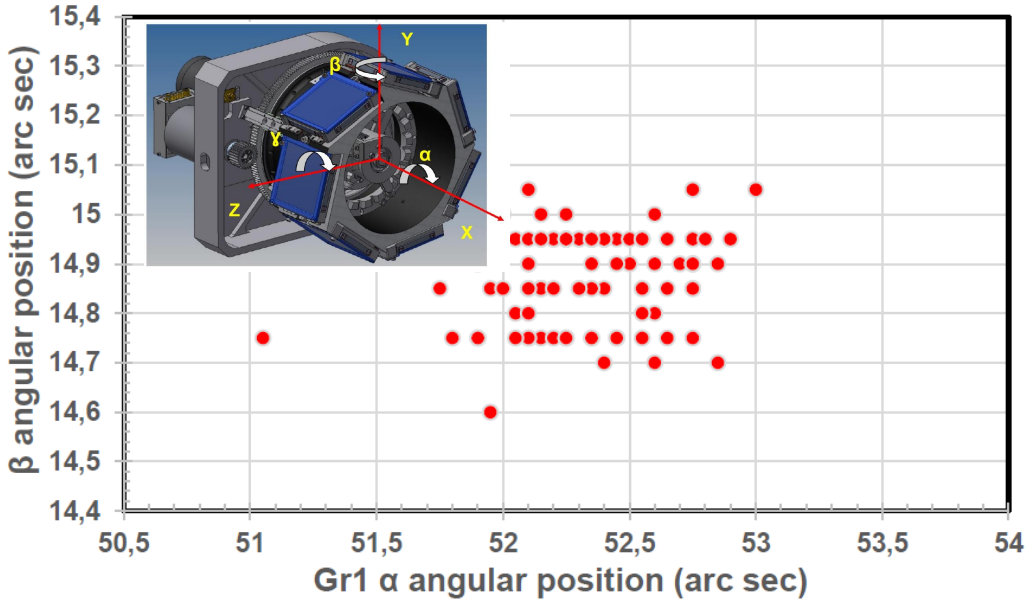

Figure 12. Results of one series of positioning reproducibility measurement.

3.3 Grating wheel in the instrument

The unit has been used intensively during the first instrument cool-downs where it has shown reliable operations. During these operation, the unit has been operated with the final instrument software which also drives automatically the locking. The feed back signal also has shown a very valuable feature.

4. CONCLUSION

The further experience with the global system test will hopefully confirm the first positive results. Even if we could have hoped to brake the barrier of the 1 arc sec positioning accuracy with the locking system, this shows again that the use of a detent/locking is one of the safest way to achieve a very high positioning accuracy. Also the mechanism used for the slit confirm that as much as it is possible a high accuracy can only be used while positioning is defined by a hard mechanical stop.

REFERENCES

[1] http://www.eso.org/sci/facilities/develop/integration/
[2] Oliva, E.; et al.; Concept and optical design of the cross-disperser module for CRIRES + instrument, SPIE, 9147-289, (2014).
[3] Lockhart, M.; et al.; Novel infrared polarimeter for the CRIRES+ instrument, SPIE, 9147-329 (2014)
[4] Seemann, U.; et al.; Wavelength calibration from 1-5 micron for the CRIRES+ high resolution spectrograph at the VLT, SPIE, 9147-208 (2014)
[5] Follert, R.; et al.; CRIRES+ a cross-dispersed high resolution infrared spectrograph for the VLT, SPIE 9147-44
[6] Brucalassi A.; et al.; Full system test and early results on preliminary acceptance Europe results for CRIRES+, SPIE, 10702-18, (2018)
[7] Dorn, R.J.; Anglada-Escude, G.; Baade, D.; et al.; CRIRES+ Exploring the cold universe at high spectral resolution, ESO The Messenger, 156 (2014)
[8] Follert, R.; CRIRES on its way, Proc. SPIE 10702-13 (2018).